THE JOURNAL OF PHYSICAL CHEMISTRY C

Article

pubs.acs.org/JPCC

Hydrophobic Surfaces: Topography Effects on Wetting by Supercooled Water and Freezing Delay

Golrokh Heydari,[†] Esben Thormann,[†,‡] Mikael Järn,[§] Eric Tyrode,[†] and Per M. Claesson*[,†,§]

[†]KTH Royal Institute of Technology, School of Chemical Science and Engineering, Department of Chemistry, Surface and Corrosion Science, Drottning Kristinas väg 51, SE-100 44 Stockholm, Sweden

[‡]Technical University of Denmark, Department of Chemistry, Kemitorvet 207, DK-2800 Kgs. Lyngby, Denmark

[§]SP Technical Research Institute of Sweden, Chemistry, Materials and Surfaces, P.O. Box 5607, SE-114 86 Stockholm, Sweden

Supporting Information

ABSTRACT: Hydrophobicity, and in particular superhydrophobicity, has been extensively considered to promote ice-phobicity. Dynamic contact angle measurements above 0 °C have been widely used to evaluate the water repellency. However, it is the wetting properties of *supercooled* water at subzero temperatures and the derived work of adhesion that are important for applications dealing with icing. In this work we address this issue by determining the temperature-dependent dynamic contact angle of microliter-sized water droplets on a smooth hydrophobic and a superhydrophobic surface with similar surface chemistry. The data highlight how the work of adhesion of water in the temperature interval from about 25 °C to below −10 °C is affected by surface topography. A marked decrease in contact angle on the superhydrophobic surface is observed with decreasing temperature, and we attribute this to condensation below the dew point. In contrast, no significant wetting transition is observed on the smooth hydrophobic surface. The freezing temperature and the freezing delay time were determined for water droplets resting on a range of surfaces with similar chemistry but different topography, including smooth and rough surfaces in either the Wenzel or the Cassie−Baxter state as characterized by water contact angle measurements at room temperature. We find that the water freezing delay time is not significantly affected by the surface topography and discuss this finding within the classical theory of heterogeneous nucleation.

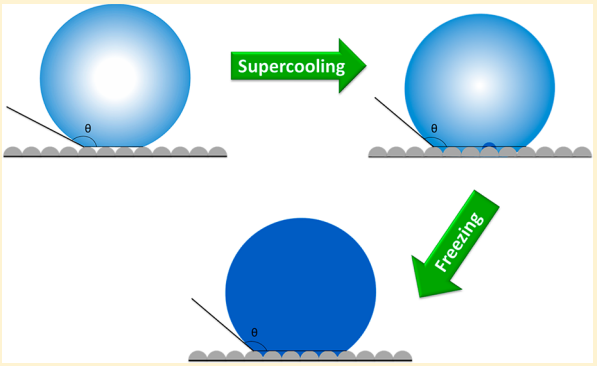

1. INTRODUCTION

Preventing ice accretion is crucial in many applications, and ice buildup triggers severe problems and safety risks in cold regions.[1−7] Numerous *active* and *passive* methodologies have been utilized to deal with icing.[8] Among the passive methods, one of the key approaches is to manipulate the surface energy of the solid to reduce the interaction with water and ice. For this reason fabrication of superhydrophobic surfaces for anti-icing applications has been an attractive topic in recent studies.[9−14] Such surfaces are not only of interest for combating icing issues, but superhydrophobic surfaces are of great interest for a variety of fundamental and industrial applications.[15−17]

For a surface to be called superhydrophobic, it is generally agreed that the contact angle should be above 150°. This can only be achieved by combining a low surface energy with topographical roughness, and both these aspects are utilized in manmade and natural superhydrophobic surfaces. It is, however, becoming increasingly clear that the wetting state of surfaces with contact angles above 150° can differ significantly, depending on how water penetrates between surfaces features with different length scales.[18] For a surface to display superhydrophobicity in the classical sense, combining high contact angle with low contact angle hysteresis and low sliding angle for water droplets, it should be in the so-called Cassie−Baxter state where no water penetration occurs between the surface topography features. This situation can be achieved either by utilizing a surface that combines a microstructure and a nanostructure or by utilizing a hierarchical surface structure.[17,19,20] On the other end of the wetting scale of a hydrophobic surface, we find the Wenzel state where the droplet completely penetrates the topographical surface features. This wetting state is characterized by high contact angle hysteresis and high sliding angle. It has been found that the multiscale surface morphology is important for inhibition of the transition from the Cassie−Baxter state toward the Wenzel state,[21] and such a transition has been described in several reports.[19,22−24]

From a wetting−icing correlation perspective, several reports have stressed ice release properties and low ice adhesion to superhydrophobic surfaces.[3,4,25−29] A comprehensive study emphasized that the ice adhesion strength measured by applying a shear force is strongly correlated to the work of

Received: May 3, 2013
Revised: September 23, 2013
Published: September 24, 2013

   dx.doi.org/10.1021/jp404396m | J. Phys. Chem. C 2013, 117, 21752−21762

adhesion as evaluated from the receding contact angle.[29] However, there are reports that criticize the low ice adhesion properties of superhydrophobic surfaces[30] or suggest criteria for these surfaces to exhibit low adhesion to ice.[31] Some reports have also discussed how frost formation is related to surface chemistry and topography, but the results reported so far are partly contradictory.[32−36] A few studies have explored the wetting behavior of surfaces at temperatures around[37,38] or below 0 °C,[39,40] which is crucial for anti-icing applications that derive benefit from surface water repellency. The correlation of kinetics of heterogeneous ice nucleation and surface properties has been considered in a few studies,[7,9,10,12,41] and there is a remaining debate on how surface roughness and wettability influence the ice nucleation process.

In this paper we systematically study the effect of temperature, ranging from ambient to temperatures well below zero, on dynamic wetting of surfaces. We utilized model surfaces with similar chemistry but tuned the surface roughness from smooth to micronano structures. The effect of condensation and/or frost formation at subzero temperatures on the hydrophobicity or superhydrophobicity of these surfaces was explored. We advocate that no single roughness parameter can be used for describing ice nucleation on rough surfaces and reach the conclusion that the surface topography has a negligible effect on the ice nucleation rate.

1.1. Theoretical Considerations on Wetting and Ice Nucleation. The Young−Dupré equation (eq 1) defines the equilibrium work of adhesion (W_e) as the free energy of making and eliminating the interface between the drop and a smooth solid surface:[29,42]

$$W_e = \gamma_{LV}(1 + \cos\theta_s) \tag{1}$$

where θ_s is the static equilibrium contact angle and γ_{LV} is the liquid surface tension. On rough surfaces, trapped air in between protrusions on the solid surface (with contact angle θ_s) assists hydrophobicity making a composite liquid−solid and liquid−air interface. The apparent contact angle, θ^*, is then commonly calculated using the Cassie−Baxter equation:[43]

$$\cos\theta^* = r_f f_s \cos\theta_s + f_s - 1 \tag{2}$$

where r_f is the roughness factor of the wet area and f_s is the fraction of the projected area of the solid surface that is wet.

In contrast, in the Wenzel state the liquid completely wets the grooves of the rough surface, and the relation between the apparent contact angle (θ^*) and the contact angle of the smooth surface (θ_s) is suggested to be given by

$$\cos\theta^* = r\cos\theta_s \tag{3}$$

where r is the real area of the surface divided by the projected surface area.[21] It should, however, be noted that the validity of the Wenzel and Cassie−Baxter equations has been questioned and the contact angle has been suggested to only be affected by the situation at the three-phase contact line and not by the interactions occurring underneath the droplet.[44] The wetting of superhydrophobic surfaces and the limits of validity of the Cassie−Baxter and Wenzel models have also been analyzed.[45]

It has been suggested to use the receding contact angle (θ_R) rather than the static equilibrium angle for calculating the work of adhesion.[46] This quantity is known as the practical work of adhesion, and it has been suggested to correlate with ice adhesion strength.[29] With this approach eq 1 is modified to

$$W_{adh} = \gamma_{LV}(1 + \cos\theta_R) \tag{4}$$

The classical theory of nucleation, developed around 75 years ago, has been used to model kinetics of heterogeneous ice nucleation considering the size of the foreign body and the contact angle between it and the ice embryo. Thermodynamic considerations show that the nucleating phase becomes stable when the sum of its bulk energy and the surface energy between the embryo and the metastable parent phase starts to decrease with increasing embryo size. This occurs when the embryo reaches a critical radius, r^*:[47]

$$r^* = -2\gamma_{12}/\Delta G_v \tag{5}$$

where γ_{12} is the embryo−parent interfacial tension, and ΔG_v is the volumetric free energy difference between the bulk embryo and the bulk parent phase that can be calculated as described in the Supporting Information. In the case of heterogeneous nucleation of supercooled water, γ_{12} is the ice-supercooled water interfacial tension, and the value of this quantity can be found in the literature (see also Supporting Information).[48]

The free energy of formation of a critical embryo (phase 2) on a spherical nucleating particle with radius r (phase 3) in the parent phase (phase 1) has been considered by Fletcher[47] and later by Liu.[49] It is given by[47]

$$\Delta G^* = \frac{8\pi\gamma_{12}^3}{3(\Delta G_v)^2} f(m, x) \tag{6}$$

where the function $f(m,x)$ considers the wetting characteristic and curvature of the convex nucleation site. It is given by[47]

$$f(m, x) = 1 + \left(\frac{1 - mx}{g}\right)^3 + x^3\left[2 - 3\left(\frac{x - m}{g}\right) + \left(\frac{x - m}{g}\right)^3\right] + 3mx^2\left(\frac{x - m}{g} - 1\right) \tag{7}$$

where

$$m = \cos\theta = \frac{(\gamma_{13} - \gamma_{23})}{\gamma_{12}} \tag{8}$$

and θ is the contact angle of the ice embryo in supercooled water on the nucleating particle, γ_{ij} is the surface free energy of the interface between phases i and j, and

$$x = r/r^* \tag{9}$$

We note that $x = \infty$ corresponds to nucleation on a flat surface and $x = 0$ corresponds to the homogeneous nucleation case. The function g is defined as

$$g = (1 + x^2 - 2mx)^{1/2} \tag{10}$$

Equations 6 and 7 describe how the free energy of formation of the ice embryo decreases with decreasing contact angle (m) and with increasing radius of the convex nucleation site (x). For concave nucleation sites, similar equations exist.[48] They read:

$$f(m, x) = 1 - \left(\frac{1 + mx}{g}\right)^3 - x^3\left[2 - 3\left(\frac{x + m}{g}\right) + \left(\frac{x + m}{g}\right)^3\right] + 3mx^2\left(\frac{x + m}{g} - 1\right) \tag{11}$$

and

dx.doi.org/10.1021/jp404396m | J. Phys. Chem. C 2013, 117, 21752−21762

$$g = (1 + x^2 + 2mx)^{1/2} \tag{12}$$

In the case of concave sites, the free energy of formation of the ice embryo, just as for convex sites, decreases with decreasing contact angle. However, for the concave sites the free energy of formation decreases with decreasing radius of the site. Thus, for a chemically heterogeneous surface ice nucleation will occur most readily on the most hydrophilic area, and for a topographically heterogeneous surface nucleation will occur most readily in concave surface sites with small radius, provided the supercooled water is able to penetrate into these depressions.

For heterogeneous nucleation of ice in supercooled water, Jung et al.[7] derived θ from Young's equation, assuming that the ice embryo contact angle in air and the water contact angle in air on the nucleating particle are the same:

$$m = \cos\theta = \frac{\gamma_I - \gamma_W}{\gamma_{IW}} \cos\theta_{WP} \tag{13}$$

where γ_I is the ice surface energy that is assumed to be constant. The value of the ice surface energy is often reported to be about 109 mJ/m^2,[50] but a value as low as 73 mJ/m^2 has also been suggested,[51] γ_W is the supercooled water surface energy,[52] γ_{IW} is the surface free energy of the interface between ice and supercooled water, and θ_{WP} is the contact angle of supercooled water on the nucleating particle.

The theory of heterogeneous nucleation, applied to ice nucleation from supercooled water, gives the rate of ice embryo formation per unit surface area and unit time as[48]

$$J_s = AT \exp\left[-\frac{\Delta g}{RT} - \frac{\Delta G^*}{kT}\right] \tag{14}$$

where T is the absolute supercooling temperature, Δg is the molar Gibbs free energy of activation for diffusion of water molecules across the water-ice boundary, R is the universal gas constant, and A has been suggested to be given by[48]

$$A = \frac{k}{h} c_{1,s} \tag{15}$$

where k is the Boltzmann's constant, h is Planck's constant, and $c_{1,s}$ is the concentration of supercooled liquid water molecules on the nucleating surface that are in metastable equilibrium with the ice embryos.

The classical heterogeneous nucleation model has been utilized in studies of how the rate of heterogeneous ice formation on macroscopic surfaces is affected by topographical features and surface chemistry. The great challenge here is to correlate the surface topography parameters to the quantities x and m, and some attempts are described in the literature.[7,9,12,53]

2. EXPERIMENTAL SECTION

2.1. Materials. Silicon wafers were cleaned with alkaline solution and then rinsed with plenty of water and analytical grade ethanol and finally dried under a stream of N_2. For preparing hydrophobic surfaces the clean wafers were modified by self-assembled monolayers (SAMs) of 1*H*,1*H*,2*H*,2*H*-perfluorooctyltriethoxysilane (Aldrich). The SAMs were formed from vapor at 70 °C, and the reaction was allowed to proceed overnight. The surfaces prepared in this way will be referred to as "smooth hydrophobic". Superhydrophobic surfaces were prepared following, with some modifications, a recently reported protocol[54] by dip coating of cleaned wafers in a homogeneous dispersion of hydrophobized fumed silica nanoparticles (AEROSIL R 972 from Evonik Industries, with average primary particle size of 16 nm) in a fluoro-polymer solution (FluoroPel PFC 604A from Cytonix). The coating was dried in air by solvent evaporation, and then the surface was calcinated at 500 °C for 2 h to increase the adhesion of the silica particles to the substrate and remove the fluoropolymer. The same silanization procedure used for preparation of the smooth hydrophobic surfaces was then utilized on these calcinated surfaces to render them superhydrophobic. This surface will be referred to as "superhydrophobic".

The same type of silicon wafer was used for preparing two additional surfaces used in the droplet freezing experiments. These surfaces were made by nanoparticle deposition followed by silane functionalization and they present the Wenzel wetting state with different roughness scales. In this case, silicon wafers were cleaned in dilute Piranha solution, followed by rinsing with water and analytical grade ethanol, and finally sonication in ethanol. These surfaces were modified by 3-aminopropyl triethoxysilane (APTES, Aldrich) utilizing a vapor phase reaction at ambient temperature overnight. The APTES silanized surfaces were rinsed with water and ethanol and then stored in pure ethanol. Electrostatic interactions between the positively charged APTES silanized surfaces and negatively charged nanoparticles facilitate deposition of the nanoparticle layers. Silica particles of 60 and 800 nm in diameter (G. Kisker GmbH, Germany), which are supplied in suspension, were first sonicated for 15 min and then diluted with water to a concentration of 0.5 mg/mL. N_2 dried silanized surfaces were dipped into the sonicated nanoparticle suspension for 10 min. The nanoparticle-coated surfaces were rinsed with water, dried with a N_2 stream, and then sintered in a furnace (Nabertherm, Germany) at 800 °C for 30 min. The surfaces were finally hydrophobized using the same procedure as previously mentioned. These surfaces will be referred to as "Wenzel hydrophobic-60 nm" and "Wenzel hydrophobic-800 nm", respectively. The water used in all cleaning and experimental works was purified with a Milli-Q Plus Unit (Millipore) and had a resistivity of 18.2 MΩ cm.

2.2. Surface Characterization. Topographical images of the surfaces were captured using an atomic force microscope (AFM) Nanoscope Multimode V (Bruker, USA) operated in Tapping Mode using Antimony doped silicon cantilevers with a tip radius of 6 nm (NSG10, NT-MDT). Roughness analysis of the AFM images was performed using nanoscope analysis (Bruker).

XPS spectra of the surfaces were recorded using a Kratos AXIS HS X-ray photoelectron spectrometer (Kratos Analytical, Manchester, UK) equipped with a monochromatic Al Kα X-ray source operated at 150 W. The pass energy for the high-resolution carbon 1s spectra was 20 eV. Quantification of atomic concentrations was made using high-resolution spectra. The high-resolution C1s spectra were fitted by considering the peak positions for carbon atoms in different binding states. The fitting was done with Origin 8.6 software, and the results are reported as peak area ratios with errors corresponding to 1 standard deviation.

2.3. Temperature-Controlled Contact Angle Measurements. Water contact angle measurements were made using a DataPhysics OCA40micro instrument (DataPhysics GmbH, Germany). The system contains a high speed CCD camera (maximum 2200 images s^{-1}) with 20 times magnification, a computer programmable droplet-dispensing unit, and a Peltier

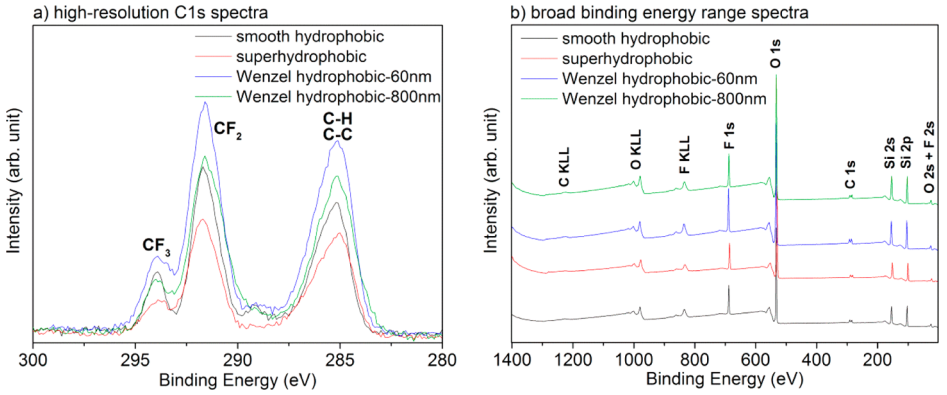

Figure 1. XPS (a) high-resolution C1s spectra. The peaks at binding energies of about 294, 292, and 285 eV are due to carbon atoms present in CF_3 groups, CF_2 groups, and carbon only bound to other carbon and hydrogen, respectively. (b) Broad binding energy range spectra of the four surfaces. The spectra have been vertically offset for clarity. The assignments of the different XPS and Auger peaks are shown in the figure.

cooling stage. Image analysis was done utilizing the SCA 20 software. It is also possible to tilt the stage that holds the surface under investigation to 90°. In order to facilitate temperature-controlled measurements, the instrument was equipped with a fast response surface temperature sensor with a flat end part. Readings were recorded by a high resolution temperature logger (TC-08, Pico Technology, UK). The surface sensor was taped firmly onto the sample surface to ensure correct readings. Drop image capturing and the surface temperature logger were started simultaneously with the same time resolution.

Static equilibrium contact angles were determined by placing the sample of interest on a cooling stage and then dispensing a 4 μL sized sessile drop on the surface. The temperature was then lowered from room temperature (~23−25 °C) to the desired subzero temperature. The relative humidity in the climate control room was about 40%.

Advancing (ACA) and receding (RCA) contact angles were measured by dispensing a 4 μL droplet and tilting the sample stage. The dispensed droplet was left undisturbed on the surface for 2−3 min to reach thermal equilibrium before evaluating the ACA and RCA from the advancing and receding side of the droplet right before it started to slide. These measurements were performed in dry N_2 atmosphere to avoid water condensation at low temperatures. For the superhydrophobic surface, above the dew point, the water droplet rolled-off upon removing the dispensing needle. In such cases, ACA and RCA were measured by continuously increasing/decreasing the volume of the initially 4 μL sized water droplet at slow speed (0.5 μL/s) until the baseline moved.

2.4. Droplet Freezing Measurements. For heterogeneous ice nucleation or freezing studies, the same DataPhysics system was equipped with two more fast response temperature sensors to monitor the temperature of the air in the vicinity of the surface and the temperature of the water droplet during the experiments.

In the freezing temperature measurements, a room temperature (about 23−25 °C) 5 μL sized water droplet was dispensed on the surface having an initial substrate temperature of ~23−25 °C. The stage was then cooled to the temperature that induced freezing of the droplet resting on the surface. Air, water droplet, and surface temperature sensors were connected to the data logger to record the corresponding temperatures. A high-speed camera captured images of the droplet during the cooling process. The freezing onset was observed as a change in the optical appearance of the droplet where it started to become hazy. This feature was used for evaluating the onset of freezing on the superhydrophobic surface where it was difficult to place the water sensor in the droplet without causing roll-off.

In the freezing delay experiments, the room temperature 5 μL sized water droplet was placed on the surfaces, and then the surface was cooled at a rate of 12−14 °C/min down to either −5 °C or −10 °C. The delay in freezing was considered as the time it took to freeze the droplet after the surface reached the target temperature.

3. RESULTS AND DISCUSSION

3.1. Surface Characterization. High-resolution XPS spectra of the C1s region as well as spectra covering the electron binding range 0−1400 eV are presented in Figure 1. The broad binding range spectra allow determination of the different elements present on the surface, whereas the high-resolution spectra provide information of the binding state of the carbon atoms in the surface region. As summarized in Table 1, XPS reveals the similar chemistry of these surfaces. For instance, the C/F ratio is in the range 0.6 ± 0.1, and the CF_2/CF_3 ratio is between 4.3 ± 0.3 and 5.2 ± 0.4 on the different types of surfaces used in this investigation.

Table 1. Surface Characteristics of the Smooth Hydrophobic, Superhydrophobic, Wenzel Hydrophobic-60 nm and Wenzel Hydrophobic-800 nm Samples

	atomic/group concentration ratio[a]		
surface	C/F	CF_2/CF_3	RMS roughness[b] (nm) for different scan sizes
smooth hydrophobic	0.6 ± 0.1	4.3 ± 0.3	0.7 (3 × 3 μm^2)
			0.85 (5 × 5 μm^2)
			1 (10 × 10 μm^2)
superhydrophobic	0.6 ± 0.1	5.1 ± 0.3	105 (3 × 3 μm^2)
			130 (5 × 5 μm^2)
			160 (10 × 10 μm^2)
Wenzel hydrophobic-60 nm	0.6 ± 0.1	4.4 ± 0.2	9 (3 × 3 μm^2)
			9 (5 × 5 μm^2)
			9 (10 × 10 μm^2)
Wenzel hydrophobic-800 nm	0.6 ± 0.1	5.2 ± 0.4	250 (10 × 10 μm^2)
			250 (20 × 20 μm^2)

[a]Derived from XPS. [b]Derived from AFM.

dx.doi.org/10.1021/jp404396m | J. Phys. Chem. C 2013, 117, 21752−21762

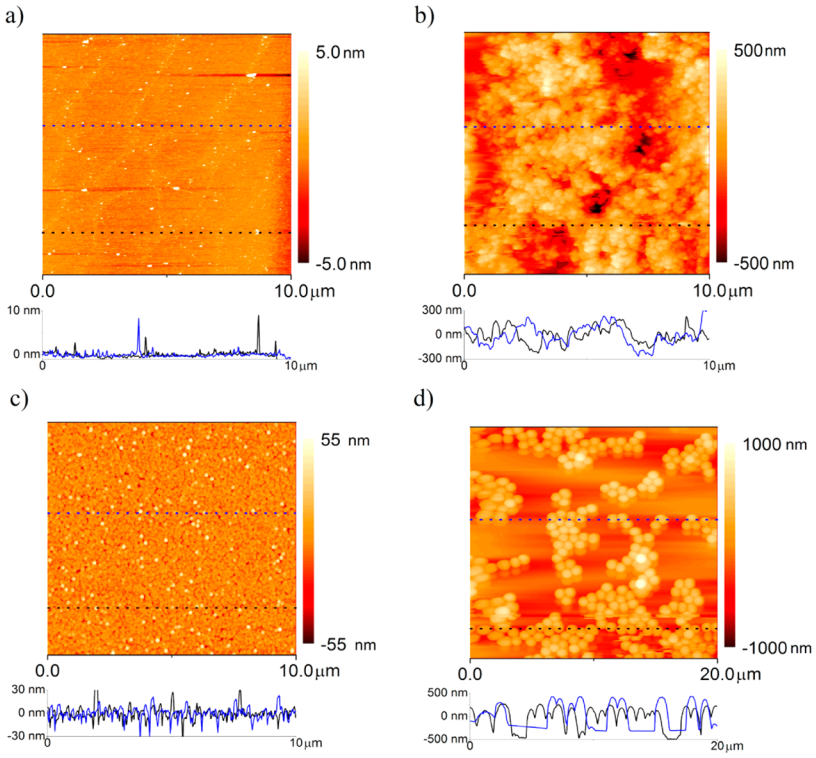

Figure 2. 10 μm × 10 μm AFM images and height profiles for the horizontal line across the scan area of (a) smooth hydrophobic, (b) superhydrophobic, (c) Wenzel hydrophobic-60 nm, and (d) 20 μm × 20 μm AFM image and height profile for the horizontal line across the scan area of Wenzel hydrophobic-800 nm surfaces.

AFM topographical images of the surfaces are shown in Figure 2. The roughness analysis of these images reported in the root-mean-square (RMS) column of Table 1 illustrates that the surface referred to as "smooth hydrophobic" has an RMS of about 1 nm, while the RMS for the superhydrophobic surface is 160 nm over a 10 × 10 μm^2 area. The "Wenzel hydrophobic-60 nm" surface has a much smaller roughness (RMS of 9 nm) than the "Wenzel hydrophobic-800 nm" with RMS of 250 nm, which is of the same order of magnitude as that of the superhydrophobic surface. A line section profile across each surface is also presented. It is obvious that the "smooth hydrophobic" surface exhibits a smooth profile with some nanometer-sized local features extending from the surface that is likely due to silane aggregate deposition.[55] In contrast, the superhydrophobic surface profile reveals peaks and valleys in the hundreds of nanometer range. The profiles shown for "Wenzel hydrophobic-60 nm" and "Wenzel hydrophobic-800 nm" reflect the packing pattern of the deposited nanoparticles where the 60 nm particles form a well-packed monolayer, whereas the 800 nm particles form a patchy layer with particle clusters separated by surface areas with no particles.

The static equilibrium and the dynamic contact angles of these surfaces, measured at 23−25 °C, are shown in Table 2. All contact angles presented are given as mean values of five measurements. For the "smooth hydrophobic" sample, the 13° contact angle hysteresis is assigned to local defects and a local agglomeration of the silanes as revealed in the AFM height image. The superhydrophobic surface has high water contact angle in addition to almost no contact angle hysteresis, demonstrating that the water droplet on this surface is in the Cassie−Baxter regime. The dimension of the contact line of the microliter-sized droplets is much larger than the roughness scale on the surface, and the surface micro/nano structures

Table 2. Water Contact Angles Measured at Room Temperature (23−25°C)

surface	static CA (deg)	ACA (deg)	RCA (deg)	hysteresis (deg)
smooth hydrophobic	100 ± 2	107 ± 2	94 ± 2	13 ± 4
superhydrophobic	161 ± 2	161 ± 2	161 ± 2	0 ± 4
Wenzel hydrophobic-60 nm	133 ± 2	137 ± 2	83 ± 4	54 ± 6
Wenzel hydrophobic-800 nm	126 ± 4	130 ± 2	92 ± 2	38 ± 4

create a composite solid/air−water contact area. The relatively large contact angle hysteresis of "Wenzel hydrophobic-60 nm" and "Wenzel hydrophobic-800 nm" surfaces reveals that water droplets on these surfaces indeed are in the Wenzel state.

3.2. Temperature Effects on Wetting. Static equilibrium water contact angles on the smooth hydrophobic and superhydrophobic samples at surface temperatures ranging from 23 to 25 °C down to −14 °C and −13 °C, respectively, are presented in Figure 3a. These data demonstrate a temperature-dependent wettability of the superhydrophobic surface, where the contact angle decreases as the temperature is lowered below 15 °C. We attribute this to condensation and, at temperatures below 0 °C, frost formation that facilitates partial spreading. However, the spreading is stochastic due to pinning of the three-phase line, and the drop in contact angle does not occur at exactly the same temperature in each experiment (but always only below 15 °C). At a surface temperature of −13 °C, the measured contact angle has decreased to 148°. The static contact angle on the smooth hydrophobic surface is practically unaffected in this temperature range.

The static work of adhesion (eq 1) is plotted in Figure 3b, using the temperature-dependent surface tension values for

dx.doi.org/10.1021/jp404396m | J. Phys. Chem. C 2013, 117, 21752−21762

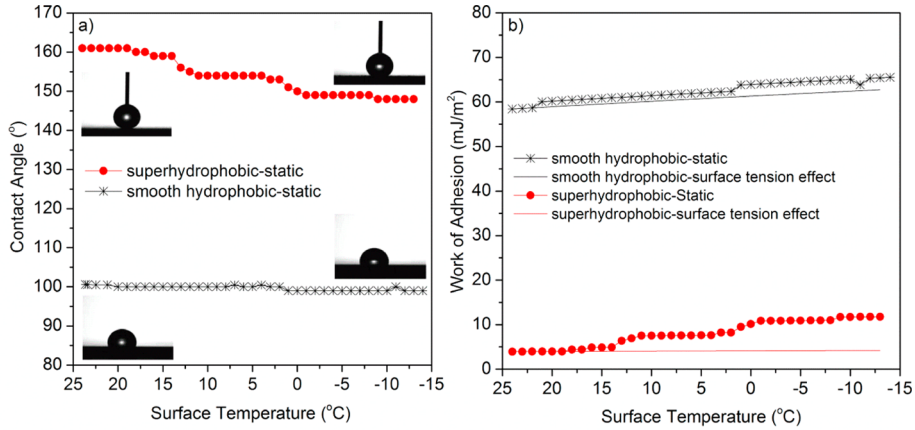

Figure 3. (a) Static contact angles on smooth hydrophobic and superhydrophobic surfaces as a function of temperature. (b) Static work of adhesion. The effect due to changes in water surface tension, for situations corresponding to temperature-independent contact angles equal to those determined at 23 °C, is shown as lines. The static contact angle and static work of adhesion were determined in ambient air with about 40% relative humidity at 23 °C.

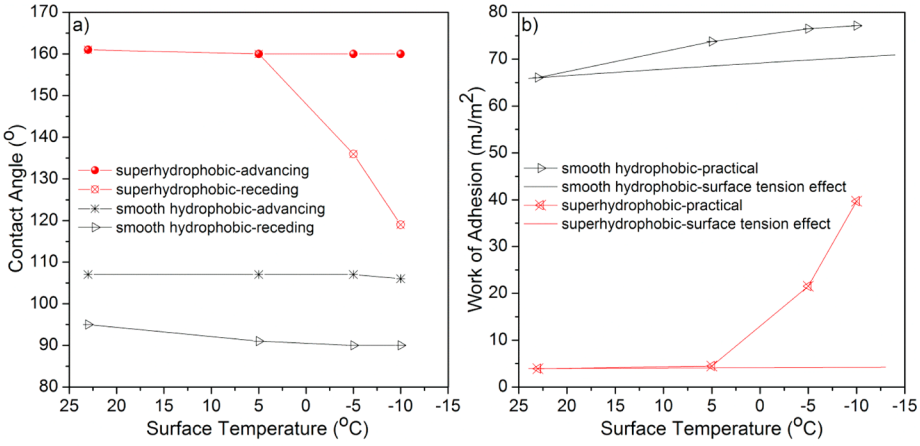

Figure 4. (a) Advancing contact angle, receding contact angle, and (b) practical work of adhesion. The effect due to changes in water surface tension, for situations corresponding to temperature-independent contact angles equal to those determined at 23 °C, is shown as lines. The advancing contact angle, receding contact angle, and practical work of adhesion were determined in a dry atmosphere.

water reported in the literature.[52] Previous studies have correlated the work of adhesion of water at room temperature to ice adhesion strength.[29,56,57] Here we have considered temperatures that are more relevant, and the data presented in Figure 3b demonstrate that the work of adhesion of water increases with decreasing temperature, partly as a result of the increasing surface tension of water (lines in Figure 3b) and partly due to decreasing water contact angles.

Advancing and receding contact angles were also studied at some selected temperatures, and these are presented in Figure 4a. The dynamic contact angle measurements were carried out in a close to dry atmosphere in order to minimize frost formation, and they are consequently not directly comparable to the static angles reported in Figure 3a. We note that the receding contact angle on the smooth hydrophobic surface decreases marginally with decreasing temperature, whereas it decreases significantly on the superhydrophobic surface at temperatures below 0 °C, i.e., in the case of supercooled water droplets. In contrast, the advancing contact angles display only weak temperature dependence on both surfaces. At room temperature, the water droplet on the superhydrophobic surface is resting on a composite surface of solid and air. Upon cooling, water evaporated from the droplet condenses in the air pockets beneath the droplet, and as the temperature continues to decrease it undergoes freezing. This induces a wetting transition from the Cassie–Baxter toward the Wenzel state, leading to reduced receding contact angle and increased contact angle hysteresis. This has implications for the practical work of adhesion, which increases significantly with decreasing temperature as illustrated in Figure 4b.

From Figure 4, it is also obvious that temperature affects the wetting of the superhydrophobic surface much more than for the smooth hydrophobic surface, even though the practical work of adhesion also increases on the smooth hydrophobic surface.

3.3. Freezing of Supercooled Water Droplets during Progressive Cooling. *3.3.1. Droplet Freezing on Smooth Hydrophobic Surfaces.* The plot in Figure 5 illustrates a representative freezing measurement on the smooth hydrophobic sample where the sensor for monitoring the water temperature is placed inside the droplet and in the vicinity of the surface. Clearly, the water temperature and surface temperature are decreasing at the same rate. The temperature of the water droplet is close to that of the surface but significantly lower than that of the surrounding air (see Figure 5). Clearly, there is a temperature gradient within the droplet,

dx.doi.org/10.1021/jp404396m | J. Phys. Chem. C 2013, 117, 21752–21762

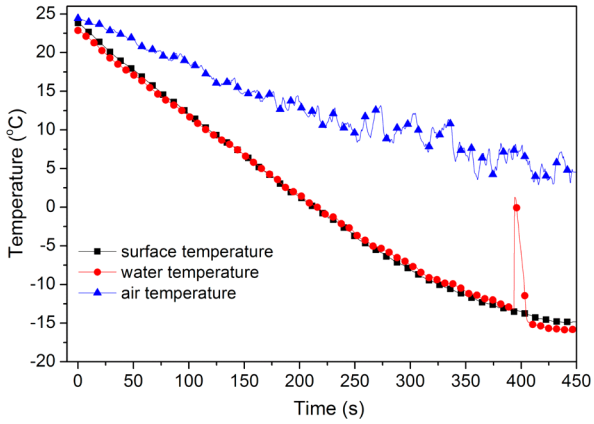

Figure 5. Freezing temperature measurement of water droplets on the smooth hydrophobic sample. The water temperature sensor is placed in the droplet from the side. The droplet was seen to freeze at a surface temperature that ranged between −14 and −22 °C, irrespective of the cooling rate which was varied between ∼5.5 °C/min and ∼13 °C/min.

and in all cases we observe that the freezing front moves from the solid−water interfaces, and once the freezing starts it is completed in about 10 ± 3 s. The sudden increase in the water temperature at the onset of freezing is due to release of the latent heat of fusion, and at *the same time* the droplet becomes hazy. Subsequently the droplet freezes while the heat is released to the substrate by conduction. The actual surface temperature at which a droplet froze varied between −14 and −22 °C for the different experimental repeats. The relatively large spread in freezing temperatures reflects the stochastic nature of the nucleation process.

3.3.2. Droplet Freezing on Superhydrophobic Surface. Water droplets on the superhydrophobic surface were found to freeze in the same temperature range as those resting on a smooth hydrophobic surface at an equivalent cooling rate. Thus, in the progressive freezing experiments, we find no indication that droplet freezing occurs less readily on the superhydrophobic surface. However, the stochastic nature of the nucleation process may prevent small effects to be noticed. For this reason we also carried out freezing delay studies, which, however, also are affected by the stochastic nature of freezing.

We note for the freezing experiment on superhydrophobic surfaces that the dispensing needle (outer diameter of 0.31 mm) was left inside the droplet in its most upper part, in order to prevent roll-off. The presence of the needle was found to have no measurable effect on the freezing temperature as determined after performing a number of systematic investigations, placing the needle at different positions inside the droplet and comparing it with the freezing temperature without the needle. Figure 6 illustrates the frames captured right before and after the onset of freezing. The freezing point is determined optically by observing changes in the light reflection from the droplet as depicted in Figure 6.

3.4. Freezing Delay of Water Droplets Held at Subzero Temperatures. The freezing delay of supercooled water droplets held at −5 °C and −10 °C on smooth hydrophobic, Wenzel hydrophobic-60 nm, Wenzel hydrophobic-800 nm, and superhydrophobic surfaces is illustrated in Figure 7. As expected, the freezing delay time is significantly longer at the higher temperature on all surfaces; i.e., the nucleation rate is faster at lower temperatures.

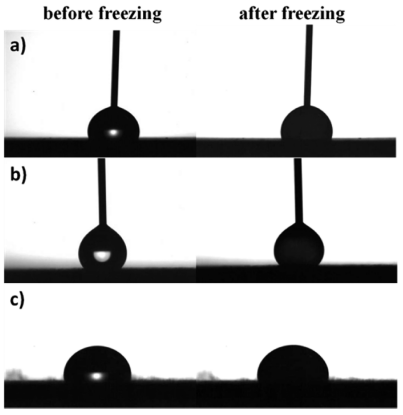

Figure 6. Images of water droplets just before and after freezing captured by a CCD camera. The droplets rest on (a) a smooth hydrophobic and (b) a superhydrophobic surface, where the needle is touching the droplet, and (c) on a smooth hydrophobic sample without the needle.

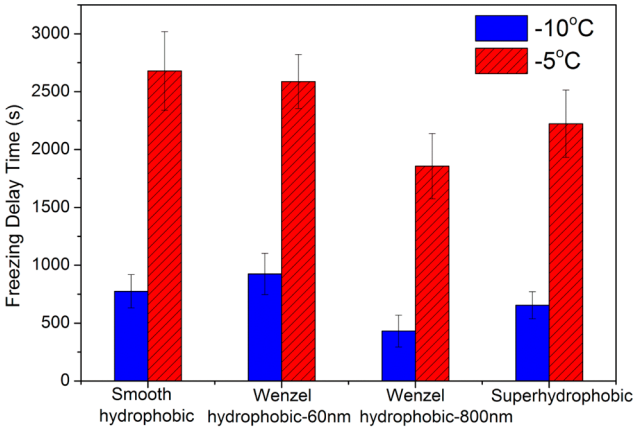

Figure 7. Delay in freezing of 5 μL supercooled water droplets measured at temperatures of −5 °C and −10 °C for the four model surfaces with similar surface chemistry but different wetting and topography characteristics. The error bar corresponds to the standard deviation.

More interestingly, at both temperatures the freezing delay is similar on all these surfaces despite their different topographical features and wettability characteristics. This is even more remarkable considering the presence of defects on the smooth surface and the aggregation of particles on the Wenzel state surfaces (see Figure 2), which could be expected to lower the energy barrier for ice nucleation and thus reduce the freezing delay time on these surfaces. Thus, the superhydrophobic surface does not retard freezing more than the smooth or the Wenzel state surfaces. Rather, the smooth surface and the Wenzel hydrophobic-60 nm surface appear to delay freezing somewhat more than the other two surfaces. These data imply that ice formation on hydrophobic surfaces under static conditions cannot be controlled by surface topography to any significant extent. We thus disregard the possibility that the small difference in surface chemistry indicated by the XPS analysis, Table 1, exactly counteracts the large difference in surface topography.

To rationalize this finding, we first consider the critical radius of the ice nucleus, r^*. Using eq 5 and the formulas provided in the Supporting Information, the value of r^* can be calculated to be 9.1 nm at −5 °C and just 4.5 nm at −10 °C. The critical ice

dx.doi.org/10.1021/jp404396m | J. Phys. Chem. C 2013, 117, 21752−21762

nucleus is clearly in contact with only a small surface area, and it is the surface energy of this surface area that is of importance for the ice nucleation. This suggests that it is the intrinsic contact angle, θ_s, and not the macroscopic contact angle, θ^*, that should be used to calculate the surface energy balance for the ice nucleus (eq 13), and it is this value of m that enters the function $f(m,x)$ described by eqs 7 and 11. The only exception to this conclusion would arise if the surface features are significantly smaller than the critical ice nucleation radius. Thus, since this is not the case for our surfaces, and they have comparable surface chemistries, the value of the interfacial energy parameter, m, is similar in all cases.

The surfaces in this study do, however, display very different roughness, which could result in different values for x (eq 9). Figure 8 illustrates how $f(m,x)$ varies with x for the case of our

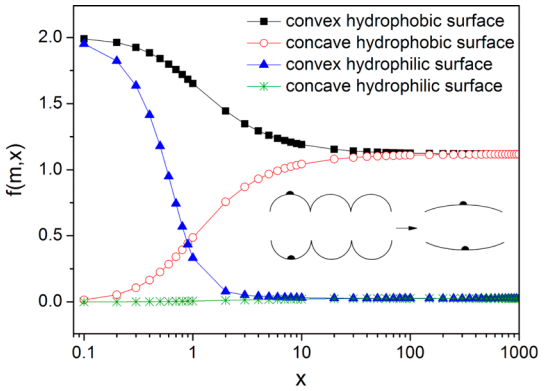

Figure 8. The function $f(m,x)$ vs the roughness parameter x (eq 9) plotted for contact angles of 94° ("hydrophobic") and 30° ("hydrophilic"). The scheme in the figure illustrates the small x (where the critical radius of ice nucleus is comparable to the size of the surface features) toward large x (where the critical radius of ice nucleus is much smaller than the size of the surfaces features), top scheme for the convex and bottom scheme for the concave surface features.

surfaces where the receding contact angle of water is about 94°, and the formal contact angle of the ice nucleus was calculated according to eq 13 using an ice surface energy of 106 mJ m^{-2}. This results in a surface energy balance for the ice nucleus in supercooled water given by $m = -0.08$. For comparison we also show the case of a hydrophilic surface where the contact angle of the ice nucleus in supercooled water is 30°, $m = 0.87$. We note that the lower the value of $f(m,x)$, the lower is the energy barrier for ice nucleation.

From the graph in Figure 8, we can draw several important conclusions. First we note that $f(m,x)$, for any value of x, decreases with decreasing contact angle of the ice nucleus, which is the basis for the assumption that hydrophobic surfaces are to be preferred over hydrophilic ones for anti-icing applications. Second, when considering convex surface features, the larger the radius of these features (the larger x, eq 9), the more readily does ice nucleate. Thus, ice nucleates more readily on flat areas than on highly convex areas. Third, the dependence of $f(x,m)$ on x for convex surface features is significant for low contact angles but rather small for high contact angles. This implies a weak dependence on surface topography for hydrophobic surfaces. Fourth, any real rough surface must by necessity have both convex and concave surface features, and ice nucleation occurs more readily in the concave features than on planar surfaces. Fifth, provided supercooled water does not penetrate concave sites on the hydrophobic surface nucleation is expected to occur most readily on the most flat regions. However, if it penetrates into the concave sites, then ice nucleation occurs most readily on these sites. This situation is promoted by frost formation or vapor condensation. Sixth, any real surface has a distribution of curvatures, and it is thus too simplistic to choose any single roughness parameter, such as RMS or R_a, to describe the surface. Rather, the ice nucleation probability will vary across the surface depending on the local nanoscale surface energy and surface curvature as depicted by the function $f(x,m)$.

Thus, for hydrophobic surfaces with similar intrinsic surface energy, as considered in this work, the topography is not expected to influence the energy barrier for ice nucleation from supercooled water significantly, unless water penetrates small concave sites where nucleation would occur more readily. With small is meant at maximum 10 times larger than the critical ice nucleus radius, as seen in Figure 8, and this critical radius is only 5−10 nm in the temperature range explored in this investigation. Thus ice nucleation is expected to occur most readily on the most flat areas, providing frost formation or vapor condensation does not increase the wettability to allow penetration of supercooled water into the small concave sites. The results shown in Figure 7, where the freezing delay time is not significantly affected by the surface topography or the wetting state, is thus to be expected when the small concave sites are not accessible for supercooled water.

Does this mean that a superhydrophobic surface does not show any benefit in anti-icing applications? Not necessarily. The droplet contact area will be lower, which reduces the nucleation rate even though the energy barrier for ice nucleation is largely unaffected compared to a flat surface with similar surface chemistry. There is also a valid kinetic argument. If the water droplet roll-off time is smaller than the freezing time, then a water droplet impinging on the surface does not have time to freeze until it has left the surface. Here, a superhydrophobic surface with a short roll-off time offers an advantage over a surface with similar chemistry but longer roll-off time. Indeed, benefits of superhydrophobic surfaces in anti-icing applications under dynamic conditions have been observed.[9,39,41,58]

3.5. Comparison with Other Studies. There are conflicting reports in the literature about the benefit of superhydrophobic surfaces in anti-icing applications. Several studies have demonstrated positive anti-icing results,[12,41] whereas other reports have shown no or limited benefits.[7,39] In two comprehensive articles, Mishchenko et al.,[41] and Alizadeh et al.[12] demonstrate that water droplet freezing is significantly retarded on superhydrophobic surfaces having well-characterized micrometer-sized surface features held in a low humidity (2−5%) environment. Alizadeh et al. conclude that the benefit arises from a combination of reduced heat transfer efficiency, smaller droplet contact area, and increased energy barrier for nucleation at a superhydrophobic surface compared to on a surface with lower contact angle. Their results contrast with our data, obtained with less ordered surfaces having smaller surface features (Figure 2b) and held at a higher humidity (40% in the measurement room, and higher close to the cool surface). In our case no significant effect on droplet freezing delay time is observed for the surfaces having different surface morphology by similar surface chemistry. Jung et al.,[7] who utilized a range of different surface chemistries and surface topographies reach the same conclusion as us, i.e., a

dx.doi.org/10.1021/jp404396m | J. Phys. Chem. C 2013, 117, 21752−21762

superhydrophobic surface does not show a significantly larger droplet freezing delay time than many other types of surfaces. A corresponding conclusion was also reached by Yin et al.,[39] performing droplet freezing experiments at a relative humidity of 80%.

There are two likely reasons for the discrepancies found in the literature. First, larger surface features, as used in experiments showing long freezing delay times,[12,41] will reduce the heat transfer more efficiently than the smaller surface features of our surfaces. Second, the long freezing delay times on superhydrophobic surfaces have been observed under low humidity conditions,[12,41] but not at higher humidities as concluded from our work and that by Yin et al.[39] Since the Cassie−Baxter to Wenzel transition is facilitated by condensation and frost formation, which will happen more readily at higher humidities, it seems plausible that this is a key difference between the two set of reports. Indeed, this suggestion finds support from measurements that demonstrate that ice accreation and ice adhesion strength on superhydrophobic surfaces increase significantly with increasing relative humidity, consistent with a Cassie−Baxter to Wenzel transition.[40] The fact that a high static water contact angle is not sufficient for judging ice adhesion strength has been emphasized, and it has been reported that small surface features are better than large ones for achieving low ice adhesion.[9] This observation has been related to the Cassie−Baxter to Wenzel transition.[58] Further studies performed under various controlled humidity conditions would shed light on whether superhydrophobic surfaces have the potential to work as anti-icing coatings under natural icing conditions.

4. CONCLUSIONS

A set of surfaces with similar surface chemistry and different surface topography and different wetting state at room temperature (Cassie−Baxter and Wenzel) has been prepared and used for studying wetting by supercooled water and droplet freezing delay. It is shown that the wetting of superhydrophobic surfaces that are in the Cassie−Baxter state at room temperature is strongly affected by temperature, and a reduction in contact angle is observed due to water vapor condensation and at lower temperatures due to frost formation. This reduction, which reveals higher adhesion of the droplet to the surface, is more pronounced for the receding contact angle. Thus, for such surfaces contact angle measurements performed at high temperature has limited value for describing the wetting of the surface by supercooled water.

The critical radius for ice nucleation is small already a few degrees below zero, in our case about 9 nm at −5 °C and 4.5 nm at −10 °C. Such a small ice nucleus will not experience either topographical or chemical variations occurring over large length scales. This leads to the conclusion that the intrinsic surface energy balance, as gauged by contact angle measurements on a flat surface, should be used in thermodynamic evaluations rather than such balances calculated based on macroscopic contact angle measurements that are affected by roughness features larger than the critical nucleus radius. The exception would be the case when the surface features are extremely tiny, significantly smaller than the critical ice nucleation radius. However, considering that the critical ice nucleation radius decreases with decreasing temperature, this seems to be a situation of more theoretical than practical interest.

For hydrophobic surfaces, only a weak dependence of surface topography on the ice nucleation rate is expected from these considerations, as also observed in this investigation. The reason is a generally weak dependence on the convex radius of surface features, as expressed in the function $f(m,x)$. Provided water vapor condensation or frost formation allows water to penetrate concave surface sites, one would expect droplet freezing to occur more readily on a rough surface than on a flat one with similar chemistry. Our results show this tendency, but the variation between the different surfaces is small, indicating that small concave sites are penetrated by water only to a limited extent. The advantage of a superhydrophobic surface for an anti-icing application may then be limited to a kinetic situation; if roll-off occurs faster than droplet freezing, then an anti-icing effect can be expected.

■ ASSOCIATED CONTENT

Ⓢ Supporting Information

Equations for calculating interfacial tension between ice and supercooled water (γ_{12} in eq 5) and volumetric free energy difference between the bulk embryo and the bulk parent phase (ΔG_v in eq 5). This material is available free of charge via the Internet at http://pubs.acs.org.

■ AUTHOR INFORMATION

Corresponding Author

*E-mail: percl@kth.se.

Notes

The authors declare no competing financial interest.

■ ACKNOWLEDGMENTS

The authors thank the Top-level Research Initiative and Nordic Innovation for financial support within the TopNano project. P.M.C, E.Ty. and E.Th. acknowledge support from the Swedish Research Council (VR).

■ REFERENCES

(1) Andersson, L.-O.; Golander, C.-G.; Persson, S. Ice Adhesion to Rubber Materials. *J. Adhes. Sci. Technol.* **1994**, *8* (2), 117−132.

(2) Laforte, J. L.; Allaire, M. A.; Laflamme, J. State-of-the-art on Power Line De-icing. *Atmos. Res.* **1998**, *46* (1−2), 143−158.

(3) Saito, H.; Takai, K.; Yamauchi, G. Water- and Ice-repellent Coatings. *Surf. Coat. Int. Part B: Coat. Trans.* **1997**, *80* (4), 168−171.

(4) Petrenko, V. F.; Peng, S. Reduction of Ice Adhesion to Metal by Using Self-assembling Monolayers (SAMs). *Can. J. Phys.* **2003**, *81* (1−2), 387−393.

(5) Kako, T.; Nakajima, A.; Irie, H.; Kato, Z.; Uematsu, K.; Watanabe, T.; Hashimoto, K. Adhesion and Sliding of Wet Snow on a Super-hydrophobic Surface with Hydrophilic Channels. *J. Mater. Sci.* **2004**, *39* (2), 547−555.

(6) Ryerson, C. C. Ice Protection of Offshore Platforms. *Cold Reg. Sci. Technol.* **2011**, *65* (1), 97−110.

(7) Jung, S.; Dorrestijn, M.; Raps, D.; Das, A.; Megaridis, C. M.; Poulikakos, D. Are Superhydrophobic Surfaces Best for Icephobicity? *Langmuir* **2011**, *27* (6), 3059−3066.

(8) Parent, O.; Ilinca, A. Anti-icing and De-icing Techniques for Wind Turbines: Critical Review. *Cold Reg. Sci. Technol.* **2011**, *65* (1), 88−96.

(9) Cao, L.; Jones, A. K.; Sikka, V. K.; Wu, J.; Gao, D. Anti-Icing Superhydrophobic Coatings. *Langmuir* **2009**, *25* (21), 12444−12448.

(10) Tourkine, P.; Le Merrer, M.; Quere, D. Delayed Freezing on Water Repellent Materials. *Langmuir* **2009**, *25* (13), 7214−7216.

(11) Sarkar, D. K.; Farzaneh, M. Superhydrophobic Coatings with Reduced Ice Adhesion. *J. Adhes. Sci. Technol.* **2009**, *23* (9), 1215−1237.

(12) Alizadeh, A.; Yamada, M.; Li, R.; Shang, W.; Otta, S.; Zhong, S.; Ge, L.; Dhinojwala, A.; Conway, K. R.; Bahadur, V.; Vinciquerra, A. J.; Stephens, B.; Blohm, M. L. Dynamics of Ice Nucleation on Water Repellent Surfaces. *Langmuir* **2012**, *28* (6), 3180−3186.
(13) Meuler, A. J.; McKinley, G. H.; Cohen, R. E. Exploiting Topographical Texture To Impart Icephobicity. *ACS Nano* **2010**, *4* (12), 7048−7052.
(14) Boreyko, J. B.; Collier, C. P. Delayed Frost Growth on Jumping-Drop Superhydrophobic Surfaces. *ACS Nano* **2013**, *7* (2), 1618−1627.
(15) Li, X.-M.; Reinhoudt, D.; Crego-Calama, M. What Do We Need for a Superhydrophobic Surface? A Review on the Recent Progress in the Preparation of Superhydrophobic Surfaces. *Chem. Soc. Rev.* **2007**, *36* (8), 1350−1368.
(16) Roach, P.; Shirtcliffe, N. J.; Newton, M. I. Progess in Superhydrophobic Surface Development. *Soft Matter* **2008**, *4* (2), 224−240.
(17) Yan, Y. Y.; Gao, N.; Barthlott, W. Mimicking Natural Superhydrophobic Surfaces and Grasping the Wetting Process: A Review on Recent Progress in Preparing Superhydrophobic Surfaces. *Adv. Colloid Interface Sci.* **2011**, *169* (2), 80−105.
(18) Feng, L.; Zhang, Y.; Xi, J.; Zhu, Y.; Wang, N.; Xia, F.; Jiang, L. Petal Effect: A Superhydrophobic State with High Adhesive Force. *Langmuir* **2008**, *24* (8), 4114−4119.
(19) Bhushan, B.; Chae Jung, Y. Wetting Study of Patterned Surfaces for Superhydrophobicity. *Ultramicroscopy* **2007**, *107* (10−11), 1033−1041.
(20) Gao, L.; McCarthy, T. J. The "Lotus Effect" Explained: Two Reasons Why Two Length Scales of Topography Are Important. *Langmuir* **2006**, *22* (7), 2966−2967.
(21) Wenzel, R. N. Resistance of Solid Surfaces to Wetting by. *Ind. Eng. Chem.* **1936**, *28* (8), 988−994.
(22) Jung, Y. C.; Bhushan, B. Wetting Transition of Water Droplets on Superhydrophobic Patterned Surfaces. *Scr. Mater.* **2007**, *57* (12), 1057−1060.
(23) Nosonovsky, M.; Bhushan, B. *Cassie-Wenzel Wetting Regime Transition Multiscale Dissipative Mechanisms and Hierarchical Surfaces*; Springer: Berlin Heidelberg: 2008; pp 153−167.
(24) Varanasi, K. K.; Deng, T.; Smith, J. D.; Hsu, M.; Bhate, N. Frost Formation and Ice Adhesion on Superhydrophobic Surfaces. *Appl. Phys. Lett.* **2010**, *97* (23), 234102−234103.
(25) Kulinich, S. A.; Farzaneh, M. Ice Adhesion on Super-hydrophobic Surfaces. *Appl. Surf. Sci.* **2009**, *255* (18), 8153−8157.
(26) Kulinich, S. A.; Farzaneh, M. How Wetting Hysteresis Influences Ice Adhesion Strength on Superhydrophobic Surfaces. *Langmuir* **2009**, *25* (16), 8854−8856.
(27) Kulinich, S. A.; Farzaneh, M. On Ice-releasing Properties of Rough Hydrophobic Coatings. *Cold Reg. Sci. Technol.* **2011**, *65* (1), 60−64.
(28) Dotan, A.; Dodiuk, H.; Laforte, C.; Kenig, S. The Relationship between Water Wetting and Ice Adhesion. *J. Adhes. Sci. Technol.* **2009**, *23* (15), 1907−1915.
(29) Meuler, A. J.; Smith, J. D.; Varanasi, K. K.; Mabry, J. M.; McKinley, G. H.; Cohen, R. E. Relationships between Water Wettability and Ice Adhesion. *ACS Appl. Mater. Interfaces* **2010**, *2* (11), 3100−3110.
(30) Chen, J.; Liu, J.; He, M.; Li, K.; Cui, D.; Zhang, Q.; Zeng, X.; Zhang, Y.; Wang, J.; Song, Y. Superhydrophobic Surfaces Cannot Reduce Ice Adhesion. *Appl. Phys. Lett.* **2012**, *101* (11), 111603−1−111603−3.
(31) Nosonovsky, M.; Hejazi, V. Why Superhydrophobic Surfaces Are Not Always Icephobic. *ACS Nano* **2012**, *6* (10), 8488−8491.
(32) Wang, H.; Tang, L.; Wu, X.; Dai, W.; Qiu, Y. Fabrication and Anti-frosting Performance of Super Hydrophobic Coating Based on Modified Nano-sized Calcium Carbonate and Ordinary Polyacrylate. *Appl. Surf. Sci.* **2007**, *253* (22), 8818−8824.
(33) Piucco, R. O.; Hermes, C. J. L.; Melo, C.; Barbosa, J. R., Jr. A Study of Frost Nucleation on Flat Surfaces. *Exp. Therm. Fluid Sci.* **2008**, *32* (8), 1710−1715.
(34) He, M.; Wang, J.; Li, H.; Jin, X.; Wang, J.; Liu, B.; Song, Y. Super-hydrophobic Film Retards Frost Formation. *Soft Matter* **2010**, *6* (11), 2396−2399.
(35) Liu, Z.; Gou, Y.; Wang, J.; Cheng, S. Frost Formation on a Super-hydrophobic Surface under Natural Convection Conditions. *Int. J. Heat Mass Transfer* **2008**, *51* (25−26), 5975−5982.
(36) Varanasi, K. K.; Hsu, M.; Bhate, N.; Yang, W.; Deng, T. Spatial Control in the Heterogeneous Nucleation of Water. *Appl. Phys. Lett.* **2009**, *95* (9), 094101−094103.
(37) Karmouch, R.; Ross, G. G. Experimental Study on the Evolution of Contact Angles with Temperature Near the Freezing Point. *J. Phys. Chem. C* **2010**, *114* (9), 4063−4066.
(38) Mockenhaupt, B.; Ensikat, H.-J. r.; Spaeth, M.; Barthlott, W. Superhydrophobicity of Biological and Technical Surfaces under Moisture Condensation: Stability in Relation to Surface Structure. *Langmuir* **2008**, *24* (23), 13591−13597.
(39) Yin, L.; Xia, Q.; Xue, J.; Yang, S.; Wang, Q.; Chen, Q. In Situ Investigation of Ice Formation on Surfaces with Representative Wettability. *Appl. Surf. Sci.* **2010**, *256* (22), 6764−6769.
(40) Kulinich, S. A.; Farhadi, S.; Nose, K.; Du, X. W. Super-hydrophobic Surfaces: Are They Really Ice-Repellent? *Langmuir* **2010**, *27* (1), 25−29.
(41) Mishchenko, L.; Hatton, B.; Bahadur, V.; Taylor, J. A.; Krupenkin, T.; Aizenberg, J. Design of Ice-free Nanostructured Surfaces Based on Repulsion of Impacting Water Droplets. *ACS Nano* **2010**, *4* (12), 7699−7707.
(42) Schrader, M. E. Young-Dupre Revisited. *Langmuir* **1995**, *11* (9), 3585−3589.
(43) Cassie, A. B. D.; Baxter, S. Wettability of Porous Surfaces. *T. Faraday Soc* **1944**, *40*, 546−551.
(44) Gao, L.; McCarthy, T. J. How Wenzel and Cassie were wrong. *Langmuir* **2007**, *23*, 3762−3765.
(45) Erbil, H. Y.; Cansoy, C. E. Range of applicability of the Wenzel and Cassie-Baxter equations for superhydrophobic surfaces. *Langmuir* **2009**, *25*, 14135−14145.
(46) Gao, L.; McCarthy, T. J. Wetting 101°. *Langmuir* **2009**, *25* (24), 14105−14115.
(47) Fletcher, N. H. Size Effect in Heterogeneous Nucleation. *J. Chem. Phys.* **1958**, *29* (3), 572−576.
(48) Pruppacher, H. R.; Klett, J. D. *Microphysics of Clouds and Precipitation*; D. Reidel Publishing Company: Dordrecht, the Netherlands, 1978.
(49) Liu, X. Y. A New Kinetic Model for Three-dimensional Heterogeneous Nucleation. *J. Chem. Phys.* **1999**, *111* (4), 1628−1635.
(50) Hobbs, P. V. *Ice Physics*; Clarendon Press: Oxford, 1974.
(51) Makkonen, L. Surface Melting of Ice. *J. Phys. Chem. B* **1997**, *101* (32), 6196−6200.
(52) Floriano, M. A.; Angell, C. A. Surface Tension and Molar surface Free Energy and Entropy of Water to −27.2 °C. *J. Chem. Phys.* **1990**, *94* (10), 4199−4202.
(53) Jung, S.; Tiwari, M. K.; Doan, N. V.; Poulikakos, D. Mechanism of Supercooled Droplet Freezing on Surfaces. *Nat. Commun.* **2012**, *3*, 615.
(54) Brandner, B. D.; Hansson, P. M.; Swerin, A.; Claesson, P. M.; Wahlander, M.; Schoelkopf, J.; Gane, P. A. C. Solvent Segregation and Capillary Evaporation at a Superhydrophobic Surface Investigated by Confocal Raman Microscopy and Force Measurements. *Soft Matter* **2011**, *7* (3), 1045−1052.
(55) Hopkins, A. J.; McFearin, C. L.; Richmond, G. L. SAMs under Water: The Impact of Ions on the Behavior of Water at Soft Hydrophobic Surfaces. *J. Phys. Chem. C* **2011**, *115* (22), 11192−11203.
(56) Murase, H.; Nanishi, K.; Kogure, H.; Fujibayashi, T.; Tamura, K.; Haruta, N. Interactions between Heterogeneous Surfaces of Polymers and Water. *J. Appl. Polym. Sci.* **1994**, *54* (13), 2051−2062.
(57) Murase, H.; Nanishi, K. On the Relationship of Thermodynamic and Physical Properties of Polymers with Ice Adhesion. *Ann. Glaciol.* **1985**, *6*, 146−149.

(58) Sarshar, M.; Swarctz, C.; Hunter, S.; Simpson, J.; Choi, C.-H. Effects of Contact Angle Hysteresis on Ice Adhesion and Growth on Superhydrophobic Surfaces under Dynamic Flow Conditions. *Colloid Polym. Sci.* **2013**, *291* (2), 427−435.